Numerical and experimental investigation of static shaft Wankel expander for compressed-air energy storage

Lomiga, Jonri; Taskin, Anil; Al-Dadah, Raya; Mahmoud, Saad; Aziz, Andrew N.

DOI:
10.1016/j.enconman.2023.117859

Document Version
Publisher's PDF, also known as Version of record

Citation for published version (Harvard):
Lomiga, J, Taskin, A, Al-Dadah, R, Mahmoud, S & Aziz, AN 2024, 'Numerical and experimental investigation of static shaft Wankel expander for compressed-air energy storage', *Energy Conversion and Management*, vol. 299, 117859. https://doi.org/10.1016/j.enconman.2023.117859

Energy Conversion and Management 299 (2024) 117859

Contents lists available at ScienceDirect

Energy Conversion and Management

journal homepage: www.elsevier.com/locate/enconman

Numerical and experimental investigation of static shaft Wankel expander for compressed-air energy storage

Jonri LomiGa [a,b], Anil Taskin [a,*], Raya Al-Dadah [a], Saad Mahmoud [a], Andrew N. Aziz [a]

[a] School of Engineering, University of Birmingham, United Kingdom
[b] Politeknik Negeri Kupang, Nusa Tenggara Timur, Indonesia

ARTICLE INFO

Keywords:
Wankel Expander
Compressed-Air Energy Storage
Design Consideration
CFD

ABSTRACT

Compressed air energy storage (CAES) is a promising technology for storing mechanical and electrical energy using the gas power cycle. The expansion device is a critical component of the CAES that determines the overall performance of the system. Standard Wankel expander (SWE) is one of the volumetric expanders which has several advantages including low vibration, ability to produce high power output, low manufacturing cost and less moving parts. However, SWE requires valves for timing the inlet and outlet flow and a balancing system to ensure reliable operation. Static shaft Wankel expander (SSWE) is an attractive solution to enable valves' removal and the need for balancing system. This paper presents a detailed experimental and numerical investigation of an SSWE performance at various operating pressures and temperatures for CAES application. An advanced computational fluid dynamic simulation model taking into account the dynamic motion of the SSWE and utilising real gas air properties. A compressed air test rig was constructed and instrumented with temperature, flow rate, pressure and torque sensors. Experimental testing at temperatures 20 °C to 80 °C and pressures of 1.5 bar_a to 3 bar_a was conducted and compared to the CFD simulations results. Correlations were developed for the friction power loss. Experimental results showed that the developed SSWE can produce power output of 504 W at 80 °C and 3 bar_a and its isentropic efficiency reached 71 % at 60 °C and 2 bar_a.

1. Introduction

The rise in energy consumption can be attributed, on the whole, to factors such as the expanding human population, expanding economies, rising levels of industrialisation, expanding transportation networks, and expanding construction activities. It is necessary to satisfy this need in a manner that does not compromise long-term viability to guarantee a profitable and secure future. In 2018, global energy statistics showed that the energy consumption was dominated by oil with 32 % followed by coal 27 % compared to other sources [1]. Also, the US energy department reported that global energy consumption was dominated by fossil fuels compared to other energy resources in the last two decades [2]. Indeed, utilizing fossil fuel to generate energy contribute to air and water pollution and climate change. Hence, more effort to reduce or even replace fossil fuel consumption by utilizing alternative energy sources that are friendly to the environment [3]. Recently, sustainable energy sources are becoming one of the solutions to overcome the dependency on fossil fuels since they can reduce the environmental impact of conventional energy sources. CAES has attracted attention of the scientific community due to many benefits [4]. Firstly, it can store significant amounts of energy for extended periods of time, suitable for meeting peak energy needs and for stabilising the power grid and can achieve efficiencies of up to 70 %, which indicates that ability to convert electrical energy into compressed air and back again with just a minimal amount of energy being wasted in the process [5]. Secondly, CAES is cost-effective when compared to other methods of energy storage such as batteries and needs a relatively low investment both to construct and maintain. CAES are versatile in that they may be installed in a broad variety of settings and can be utilised to supplement the production of energy from other renewable sources such as wind and solar [6]. For these reasons compressed air energy systems show potential for meeting the growing need for energy while also facilitating the shift towards a more sustainable energy future.

Numerous research has been carried out to develop compressed air systems for various applications such as cooling [7], cryogenic [8], energy storage [9,10] automotive [11,12,13,14] renewable energy [15] and micro grid electricity [16]. In the compressed air systems, the expander plays a crucial role as it determines the performance of the

* Corresponding author.
E-mail address: anil.taskin@yahoo.com (A. Taskin).

https://doi.org/10.1016/j.enconman.2023.117859
Received 7 August 2023; Received in revised form 3 November 2023; Accepted 4 November 2023
Available online 19 November 2023

Table 1
Research development of expansion device for CAES.

Ref	Expander	Application	Operating Conditions	Performance
[24]	Piston Expander	CAES	3—6 bar_a	57 % 581 W
[20]	Single Screw Expander	CAES	12—16 bar_a	65 % 40 kW
[19]	Single Screw Expander	CAES	4—16 bar_a	55 % 22 kW
[18]	Single Screw Expander	CAES	9 bar_a	65.9 % 8.8 kW
[22]	Scroll Expander	CAES	4 – 7 bar_a	73.5 %2.25 kW
[23]	Scroll Expander	CAES	3.75 bar_a	69 % 1073 W
[27]	Axial turbine	CAES	2 bar_a	47.1 % 630 W
[40]	SWE	CAES	4 – 6 bar_a	87 % 8.5 kW
[3837]	SWE	CAES	3—5 bar_a	70 % 10 kW
[43]	SSWE	CAES	2 bar_g	64.88 % 100 W
[26]	Radial inflow turbine	CAES	3.5 bar_g	76.7 % 3.3 kW
[44]	SWE	CAES	6 bar_g	77 % 4.75 kW
[39]	SWE	CAES	5 bar_a	87 % 50 kW
Current	SSWE	CAES	3 bar_a	67 % 504 W

system in terms of power output and efficiency [10,17]. Many researchers have investigated various types of expanders for compressed air systems. Zhi et al. [18] experimentally tested single screw expander using centrifugal and filter-oil gas separator to study the performance of the expander. They achieved a cycle efficiency of 65.9 % using the centrifugal oil–gas separator which is 1.42 times higher than that with the filter oil–gas separator and concluded that there is a potential to use centrifugal gas separator in the compressed air application to improve the performance of the screw expander. He et al. [19] developed a test rig to investigate the performance of screw expander in terms of power output and cycle efficiency using compressed air. They investigated the effect of flow rate, inlet and outlet temperature, rotational speed, and inlet pressure showing that the expander has good performance at high inlet pressure and high rotational speed. The maximum power output reached 22 kW and the maximum cycle efficiency of 55 % was obtained. Lu et al. [20] performed experimental study of compressed air screw expander for refrigeration application with the expander rotor diameter of 175 mm. The results showed that the screw expander can be used for the refrigeration application as it provided a maximum COP of 0.9.

Other researchers have focused on developing scroll expander for compressed air systems. Xinghua et al. [21] developed a numerical model of scroll expander using MATLAB software to investigate means of improving its energy conversion efficiency. They evaluated the performance of the scroll expander using several parameters such as the volume, mass, pressure, and temperature of air inside its chambers. The results indicated that at inlet air pressure between 0.35—0.65 MPa, the energy conversion efficiency obtained is between 23 % and 26 %. Also, the torque and efficiency modelling results exhibited a good agreement with the experimental results. Zhang et al. [22] developed a scroll expander model and validated it against experimental results. A numerical model is used to optimize the expander performance in terms of pressure ratio, inlet temperature, clearance size, and scroll height to pitch ratio. They concluded that the results of the numerical model are in good agreement with the experiment results, hence these parameters can be used to design the scroll expander for compressed air application. Guangbin et al. [23] developed a numerical model that takes into account suction, leakage, heat transfer and discharge losses and validated it against experimental results. Their results showed that the power output increased as the rotational speed increased. The simulation results of rotational speed agreed well with the experimental results in the range between 1740—2340 rpm. Furthermore, the expander volumetric efficiency reached 69 % when the clearance of 0.04 mm was used.

The other type of expander that was developed for compressed air is reciprocating piston expander. Tenissara et al. [24] experimentally tested a small-single piston expander for compressed air and evaluated its performance in terms of mass flow rate, the torque and rotational speed at inlet pressure ranging from 3 to 6 bar. They obtained maximum power of 581 W with the maximum rotational speed of 710 rpm. Also, the expander achieved maximum isentropic efficiency of 61 % at inlet pressure of 3 bar. The experimental results indicated that increasing the speed resulted in increasing the mass flow rate. Huang et al. [25] tested experimentally a piston engine for compressed air application at inlet pressure between 5 bar and 9 bar absolute. Their results showed maximum power output of 0.95 kW at inlet pressure of 9 bar and

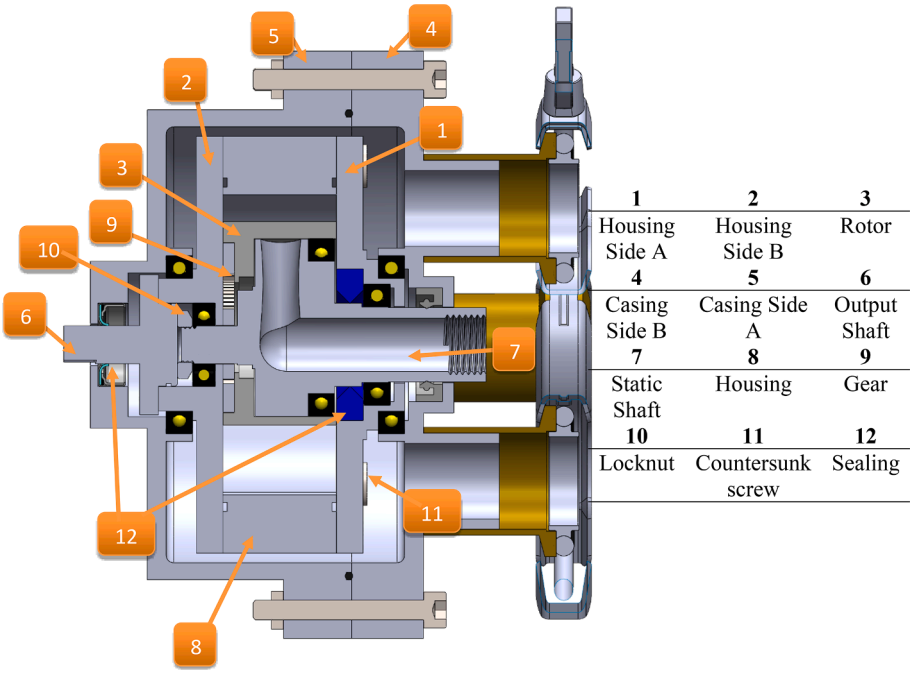

Fig. 1. Section view of the SSWE assembly.

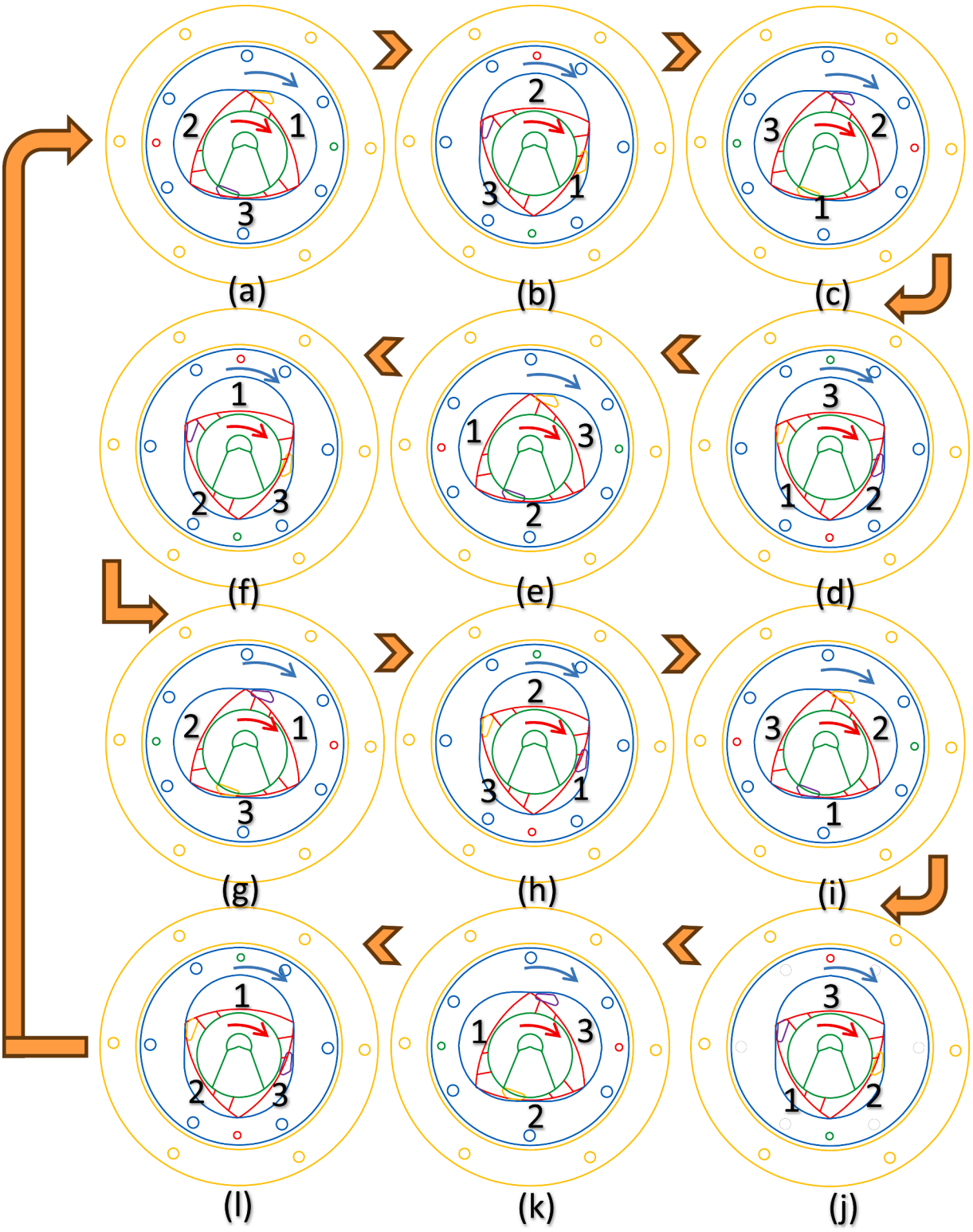

Fig. 2. Operational cycle of a SSWE with three pairs of expansion chambers.

rotational speed of 1320 rpm thus proving that the expander can be used for automotive applications.

Regarding the velocity type expanders, Al Jubori et al. [26] studied radial-inflow turbine for small-scale compressed air application. They integrated mean-line modelling with 3D CFD simulations and showed that the maximum power output, isentropic efficiency, and the system efficiency achieved are 3.282 kW, 76.70 % and 12.46 % respectively. Khalil et al. [27] developed a numerical simulation of a small scale axial turbine and experimentally tested it to investigate its performance in a compressed air open-system. In the numerical model, they used ANSYS CFX software to simulate the fluid behavior in the turbine passage and predict the performance of the turbine. Their experimental results showed that the maximum power output of 796.89 W can be reached with isentropic efficiency of 47.1 %. The numerical results were

Table 2
Working principles of SSWE.

	Chamber 1	Chamber 2	Chamber 3	Rotor Angle °	Housing Angle °	Output Shaft Angle °
a	Exhaust	Expansion	Suction	0 or 720	0 or 1080	0 or 1080
b	Exhaust	Expansion	Suction	60	90	90
c	Suction	Exhaust	Expansion	120	180	180
d	Suction	Exhaust	Expansion	180	270	270
e	Expansion	Suction	Exhaust	240	360	360
f	Expansion	Suction	Exhaust	300	450	450
g	Exhaust	Expansion	Suction	360	540	540
h	Exhaust	Expansion	Suction	420	630	630
i	Suction	Exhaust	Expansion	480	720	720
j	Suction	Exhaust	Expansion	540	810	810
k	Expansion	Suction	Exhaust	600	900	900
l	Expansion	Suction	Exhaust	660	990	990

validated against experimental results in terms of both power output and efficiency with maximum deviation of 12 % and 16 % respectively.

In recent years, there has been extensive research on Wankel rotary engine because of its potential to be used in different applications such as pumps [28], compressors [29,30] internal combustion engines [31,32,33,34] and as expanders. SWE has advantages over others due to being more compact, having low noise, less vibrations, simple construction as it has two major components and low manufacturing cost [35,36]. Furthermore, SWE can be used for small-scale power output applications (5—–20 kW). Numerous research has been reported on the development of Standard Wankel as an expansion device. Badr et al. [35] conducted research regarding positive displacement expanders for low power output using steam as working fluid. They compared turbine, rotary vane, rotary piston, screw expanders and SWE for small-scale combined heat and power (CHP) application. Their results indicated that all positive displacement expander types had more advantages compared to turbine and reciprocating-piston expanders. Also, they recommended SWE as more suitable for this CHP application compared to other expansion devices. However, it required some modifications related to intake and exhaust ports in order to be used in this application. Furthermore, they also found that the turbine is more expensive and more complex to manufacture for the small-scale CHP application. Badr et al. [36] also developed SWE as an expansion device using steam as working fluid for Rankine cycle application. They used original rotary engines by Mazda and Curtiss - Wright with the boiler inlet pressure from 4 – 10 bar, inlet temperature between 200 and 350 °C and the condenser pressure of 1.25 bar. They evaluated the performance of the expanders based on pressure ratio (Mazda = 5—–6, Curtiss-Wright = 4.5—–5.25) and concluded that both expanders can be used for low power output of 5 – 20 kW with rotational speed of 3000 rpm for Mazda rotary engine.

Antonelli et al. [37] evaluated the feasibility of using Standard Wankel expander in low temperature organic Rankine cycle where six working fluids (R236ea, R600, R600a, R-601, R-245ca, R245fa) have been studied. Isentropic efficiency was chosen as the main parameter to compare the working fluids performance. Numerical modelling was carried out using AMESim software to simulate the in-chamber pressure with respect to inlet and outlet and the volume of chambers. The model was then validated using experimental testing with working conditions (inlet temperature = 80 – 120 °C, inlet pressure = 3 – 5 bar, rotating speed = 500 – 1500 rpm) and used to evaluate the expander performance. Results showed that among the working fluids, R600 and R601 achieved the best isentropic efficiency of around 86 % and 85 % respectively. Antonelli et al. [38] have also investigated experimentally and numerically the influence of valve timing on the performance of the SWE. In the experiments, they measured the torque, working fluid mass flow rate and indicated power output at varying inlet pressure of 3 – 5 bar and rotational speed of 500 to 1500 rpm. Numerical modelling using AMESim was chosen to predict the expander performance with R152a and R600a as working fluids at the temperature range 100 – 120 °C. It was found that the best performance was achieved with intake valve timing ranging from 0 to 8° and exhaust valve timing of 25 – 35°. Moreover, R600a achieved the highest isentropic efficiency of around 95 % while R152a achieved around 90 % at temperature of 110 °C. Regarding the cycle thermal efficiency, both working fluids showed quite similar value of about 7 %.

Francesconi et al. [39] developed a numerical model of SWE taking

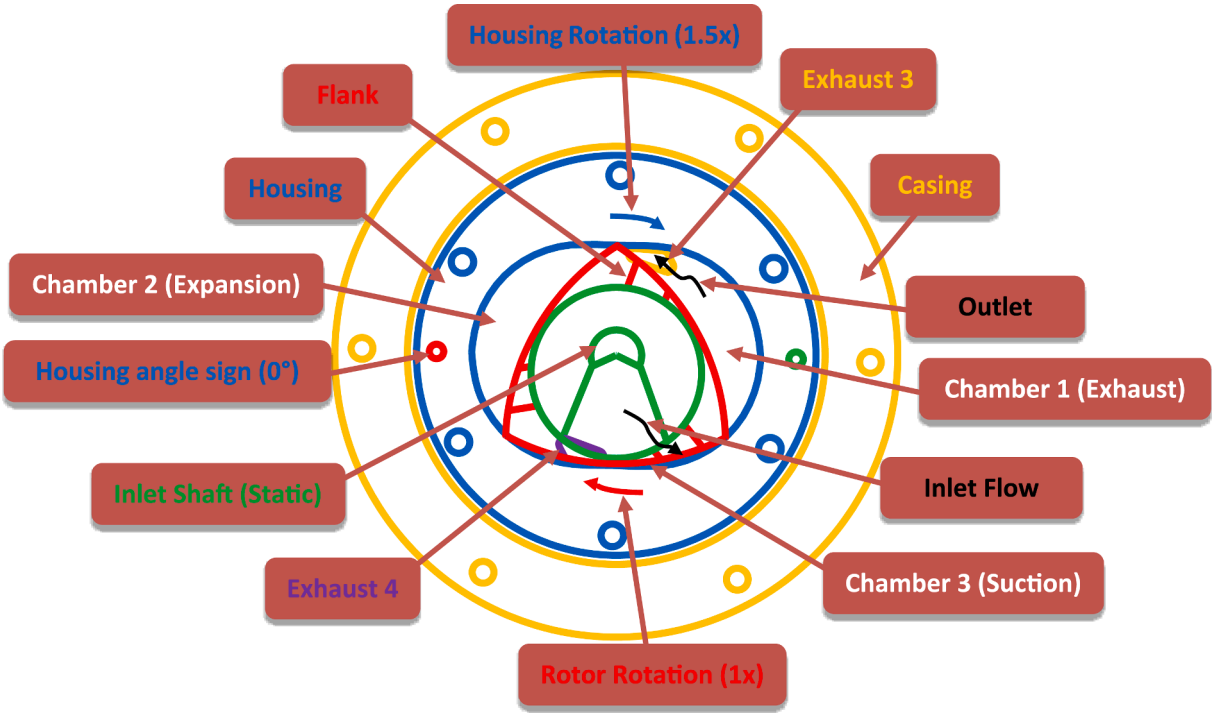

Fig. 3. The main flow passage in SSWE.

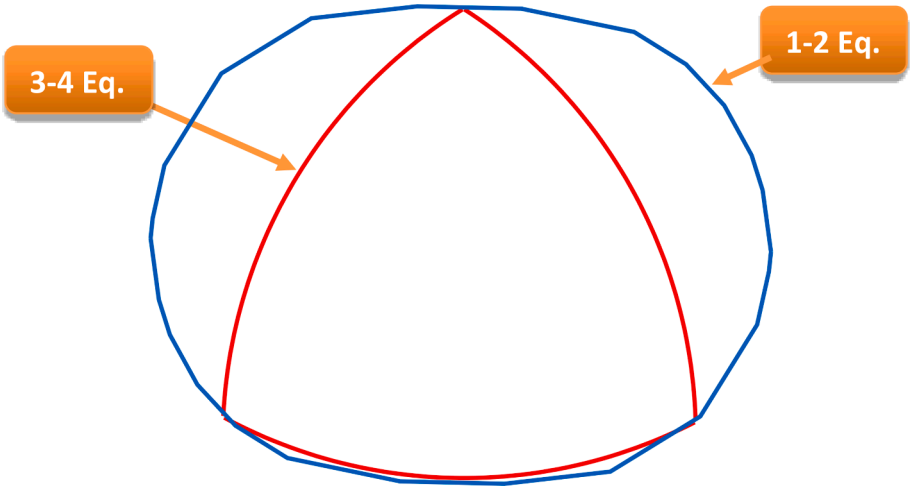

Fig. 4. The Geometry of Static Shaft Wankel Expander.

Table 3
Specifications of Static SSWE.

Parameter	Value mm	Abbreviation
Eccentricity	4.8	e
Radius	35	r
Clearance	0.1	c
Rotor flanks radius	60	f
Width of expander	32	w

fluid dynamic and mechanical losses into account to obtain its power output and isentropic efficiency for CAES. Their results indicated that the highest isentropic efficiency achieved was 87 % at rotating speed of 1250 rpm meanwhile 59 % was the lowest isentropic efficiency with rotating speed of 500 rpm. Sadiq et al. [40] investigated single and two-stage rotary SWE using 3D CFD modelling and studied the effect of different parameters namely port size, port spacing on the expander power output and isentropic efficiency using air as the working fluid. They used port spacing ranging from 28 mm to 66 mm and port diameter ranging from 15 mm to 50 mm. Also, they used various expander sizes (r = 48, e = 6.6, b = 32) mm and (r = 58, e = 8, b = 40) mm which were implemented for both configurations. Results showed that power and isentropic efficiency of two-stage configuration are higher than single-stage achieving 91 % with 8.52 kW and 87.25 % with 4.75 kW respectively at the operating conditions (inlet temperature = 400 K, inlet pressure = 6 bar, rotating speed = 7500 rpm). Furthermore, they showed the disadvantage of using SWE as it needs balancing to stabilize when it is connected to the system and also original Wankel engine required valves for use as SWE [41]. Tozer et al. [42] developed 3D CFD numerical simulation of Standard Wankel expander for air liquefaction applications and investigated the effect of apex gap size (0.05 mm, 0.1 mm and 0.25 mm) on its performance. They compared single and double ports for inlet and outlet to predict the power output and isentropic efficiency. The numerical simulation showed that at the rotational speed of 6000 rpm, SWE with double port achieved highest power output of 385 W. The highest isentropic efficiency of 64 % was obtained at inlet pressure of 2 bar and rotational speed of 1200 rpm.

Although some researchers have investigated SWE, however, a major disadvantage of such expander is that it needs valves to control the timing of the inlet and outlet flow. For micro-scale of CAES, SSWE is an attractive solution to compensate for valves removal [42,43] however, there is limited research on SSWE for compressed air application. Although the performance of other expanders for CAES application has been investigated, there is lack of literature regarding the SSWE as shown in Table 1. In this paper, a significantly improved design of the SSWE concept developed by [43], was manufactured, experimentally tested and numerically modelled to investigate its performance at wide range of inlet temperature and pressure conditions for CAES application. Also, the paper describes the development of an advanced CFD model for the SSWE taking into account the complex dynamic motion of the rotor and the real fluid properties by integrating REFPROP thermodynamic software to the CFD model.

2. Static shaft Wankel expander operation and geometry

SSWE is derived from the DKM (Drehkolben Maschine), which has a similar principle of operation as the first prototype of rotary Wankel engine. However, in order to be used as an expander, it required modifications of the inlet and outlet ports [31], and the removal of the spark plug. In DKM, the shaft and the rotor are a single part, whereas in SSWE, the shaft is static with the help of bearing and the rotor can rotate. The SSWE consists of a housing with epitrochoid shape, triangle rotor, shaft and ports for the fluid inlet and outlet. In this SSWE, there is no valve mechanism and it can transmit its power output by the rotary motion of the rotor allowing it to be more compact and more simply constructed than the reciprocating engine. Fig. 1 shows a section view of the SSWE assembly.

The operation of the SSWE is based on volumetric expansion process where a pressurised gas expands as it passes through the chambers producing power output. In more detail, the air enters the chamber 3 through the flank which is the hole inside of the rotor then it will expand as the chamber volume increases due to the rotation of the rotor and the housing at the same time as shown in Fig. 2a**.** The pressurized gas in chambers 2 and 3 rotates the rotor and housing. During rotation, gas is expelled from the yellow exhaust port along with the decreasing volume of chamber 1. At this time, the purple exhaust port is blocked by the side of rotor. Since the rotor and the housing are connected with a 3:2 ratio gear, the housing rotates 90 degrees while the rotor rotates 60 degrees as shown in Fig. 2b**.** The rotational speed difference between the rotor and the housing causes displacement. Table 2 shows the process of all chambers and the angle that each part rotates. The timing of inlets and outlets as valves is automatically controlled by exhaust port geometry.

When the rotor completes two full turns and the housing completes three turns, it returns to initial position as shown in Fig. 2a**-l.** In all cases, one chamber is in suction process, the other is in expantion process and the last is in exhaust process. Outlet port should be open when the expansion chamber reach the maximum volume and should be close when the suction chamber reach the minimum volume as shown in Fig. 2d**-g.** Outlet ports should be as large as possible to achieve high efficiency [41]. After Fig. 2l, SSWE completes the rotation cycle and all

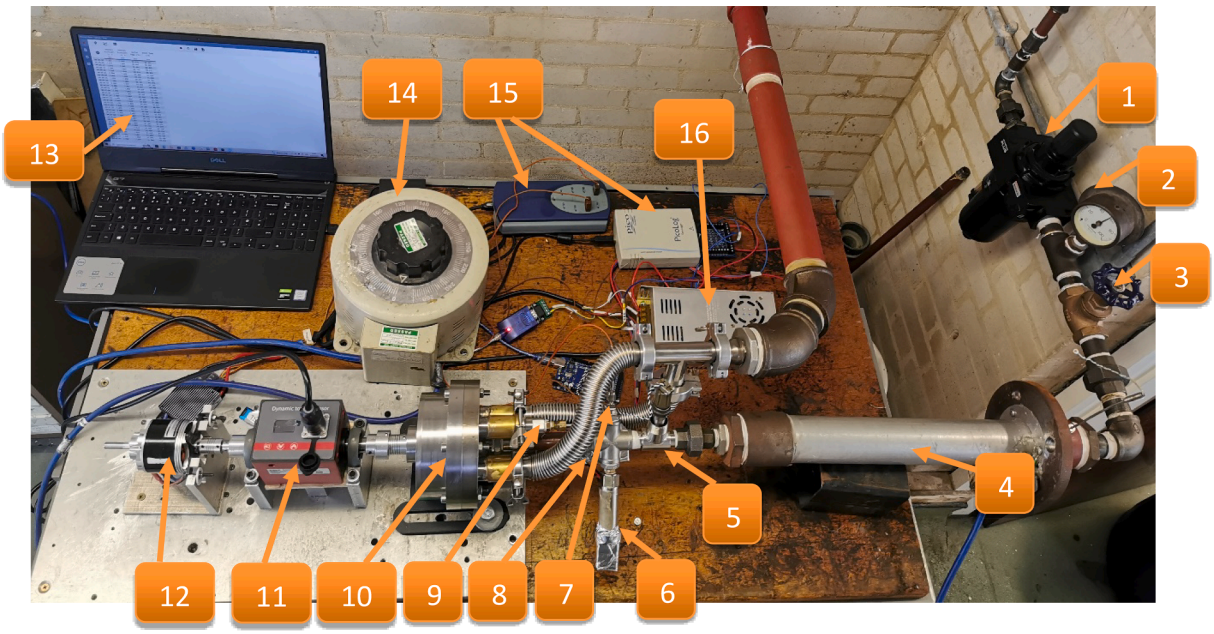

1	2	3	4
Pressure Regulator	Pressure Gauge	Globe Valve	Heater
5	**6**	**7**	**8**
Flow Meter	Inlet Pressure Transducer	Inlet Thermocouple	Outlet Pressure Transducer
9	**10**	**11**	**12**
Outlet Thermocouple	SSWE	Torque Meter	Generator
13	**14**	**15**	**16**
Computer	Heat Controler	DataTaker	Power Supply

Fig. 5. Test Rig.

chambers complete suction, expansion and exhaust processes. This will cause the rotation of the rotor producing power output through the output shaft connected to the housing. When the housing is rotating with the help of the gear, timing of the inlet and outlet flow can be controlled thus there is no need for inlet and exit valves like in the Standard Wankel engine. To increase the flow port area, there are four outlet ports in housing sides.

A novel volumetric expander, details of its inlet, outlet and their connection to the main flow passage are listed in Fig. 3.

The important geometric parameters of the Wankel expander are eccentricity e and the generating rotor radius r. The ratio of the generating rotor radius to the eccentricity is called the trochoid constant K, which will provide a typical index for trochoid to indicate its geometric configuration. The geometry of Wankel expander can be expressed based on the following equations:

The housing shape as shown in Fig. 4 can be generated using equations (1) and (2) [36,45]:

$$x_h = e\cos 3\theta + r\cos\theta \tag{1}$$

$$y_h = e\sin 3\theta + r\sin\theta \tag{2}$$

Where e, r, θ are eccentricity, rotor radius and eccentricity rotation angle respectively.

The equation of rotor and housing shown in Fig. 4, is given as [36,45]

$$x_r = r\cos 2v + \frac{3e^2}{2r}(\cos 8v - \cos 4v) \pm e\left(1 - \frac{9e^2}{r^2}\sin^2 3v\right)^{\frac{1}{2}}(\cos 5v + \cos v) \tag{3}$$

$$y_r = r\sin 2v + \frac{3e^2}{2r}(\sin 8v - \sin 4v) \pm e\left(1 - \frac{9e^2}{r^2}\sin^2 3v\right)^{\frac{1}{2}}(\cos 5v + \cos v) \tag{4}$$

Where the intervals v is given by:

$$v = \left[\frac{\pi}{2}, \frac{5\pi}{6}\right], \left[\frac{11\pi}{6}, \frac{13\pi}{6}\right], \left[\frac{19\pi}{6}, \frac{21\pi}{6}\right] \tag{5}$$

Table 3 lists the dimensions of the Wankel expander studied in this work.

3. Experimental work

To investigate the performance of the developed SSWE, experimental testing was carried out using the compressed air test rig shown in Fig. 5. The test rig consists of compressed air source, pressure regulator, globe valve, heater, SSWE (see Fig. 6) and torque meter. The compressed air passes through inlet pipe connection to the SSWE causing the rotor and housing to rotate.

The pressure regulator is used to setup the inlet pressure (1.5, 2, 2.5 and 3 bar_a) and the heater is used to control the air temperature using a

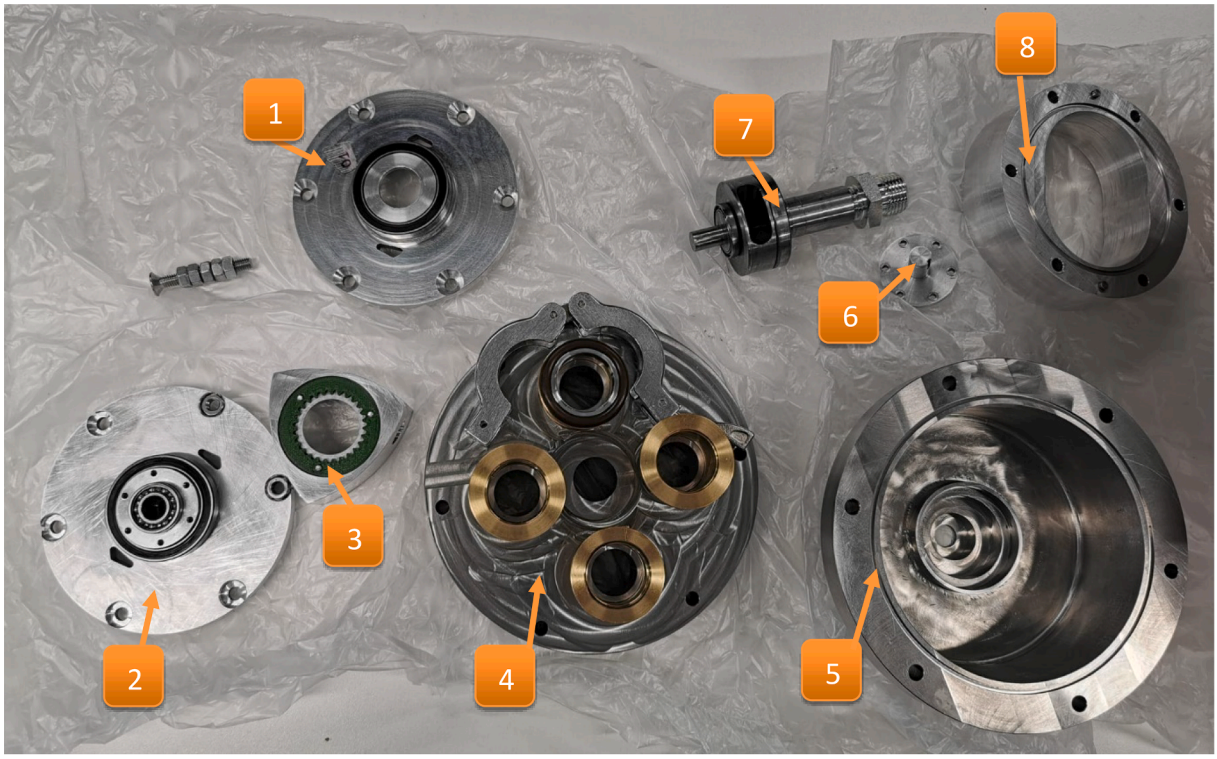

1	2	3	4
Housing Side A	Housing Side B	Rotor	Casing Side A
5	**6**	**7**	**8**
Casing Side B	Output Shaft	Static Shaft	Housing

Fig. 6. Exploded diagram of the SSWE.

voltage regulator. The test rig is equipped with various measuring devices including an Omega FTB-933 gas turbine flow meter with a measurement range of 1-10ACF was used and connected to the Arduino mega-2560 to record the mass flow rate data. Two pressure transducers are used to measure inlet and outlet pressure and thermocouples of types K were connected to the inlet and outlet of SSWE to measure inlet and outlet temperatures during the experimental testing. The pressure and temperature data were recorded using Picologer software installed on a computer and saved in excel csv file. Rotary torque sensor type DYN-200—10 N.M with capacity of 10 N.m and output signal of ± 5 V was used to measure the rotational speed and output power.

Fig. 7a shows the results of the experimental testing of the SSWE obtained at various air inlet pressure and inlet temperature. It shows that the power output increases with the increase in inlet pressure and inlet temperature where at the maximum pressure of 3 bar_a and maximum inlet temperature of 80 °C, 504 Watts were produced. As for the isentropic efficiency of the SSWE, Fig. 7b shows that the efficiency decreases after 2 bar_a.

The advantage of using Static shaft Wankel expander is that there is no adding valve in the inlet as the static shaft can control the inlet flow and reducing the complexity of design. Another advantage is that there is no need to add mass balancing as the author [41] did since rotor and housing rotated based on their centre of mass leading to dynamically balanced of those parts.

The results of this SSWE is compared with other expander in Table 1.

Two main performance parameters are the power output and the isentropic efficiency that are used to analyse the SSWE performance. Equations below describe calculation of the power output and isentropic efficiency of the expander from sensors of the test rig.

$$\eta = \frac{P_{actual}}{P_{ideal}}$$

P_{ideal}, which is isentropic power, is calculated according to enthalpy change and mass flow rate.

$$P_{ideal} = \dot{m}_{inlet}(h_{inlet} - h_{outlet})$$

Leakage is between rotor and housing due to apex clearance. Although static shaft wankel is completely sealed away from the environment, with the casing as displayed in Fig. 1. Hence inlet mass flow rate and outlet mass flow rate are equal.

P_{actual}, which is the output shaft power, is read from the torque meter. Torque meter calculates the output power according to torque and rpm.

$$P_{actual} = \frac{T_{Shaft} RPM}{9548.8}$$

Both $\dot{m}_{inlet}$ and h_{inlet}, h_{outlet} are written to excel file. Flow meter, temperature sensor and pressure transducers are connected with Arduino. Stream Data from Arduino into Excel connected by Refprop to get the enthalpy from pressure and temperature value. In order to maintain the steady flow in test data, collecting data is started 5 min after the changed the pressure or temperature for every experiment. Influence of unsteady flow on test data is only 1 % due to sensor accuracy.

In the experiments, test rig was run 10 to 15 min before data

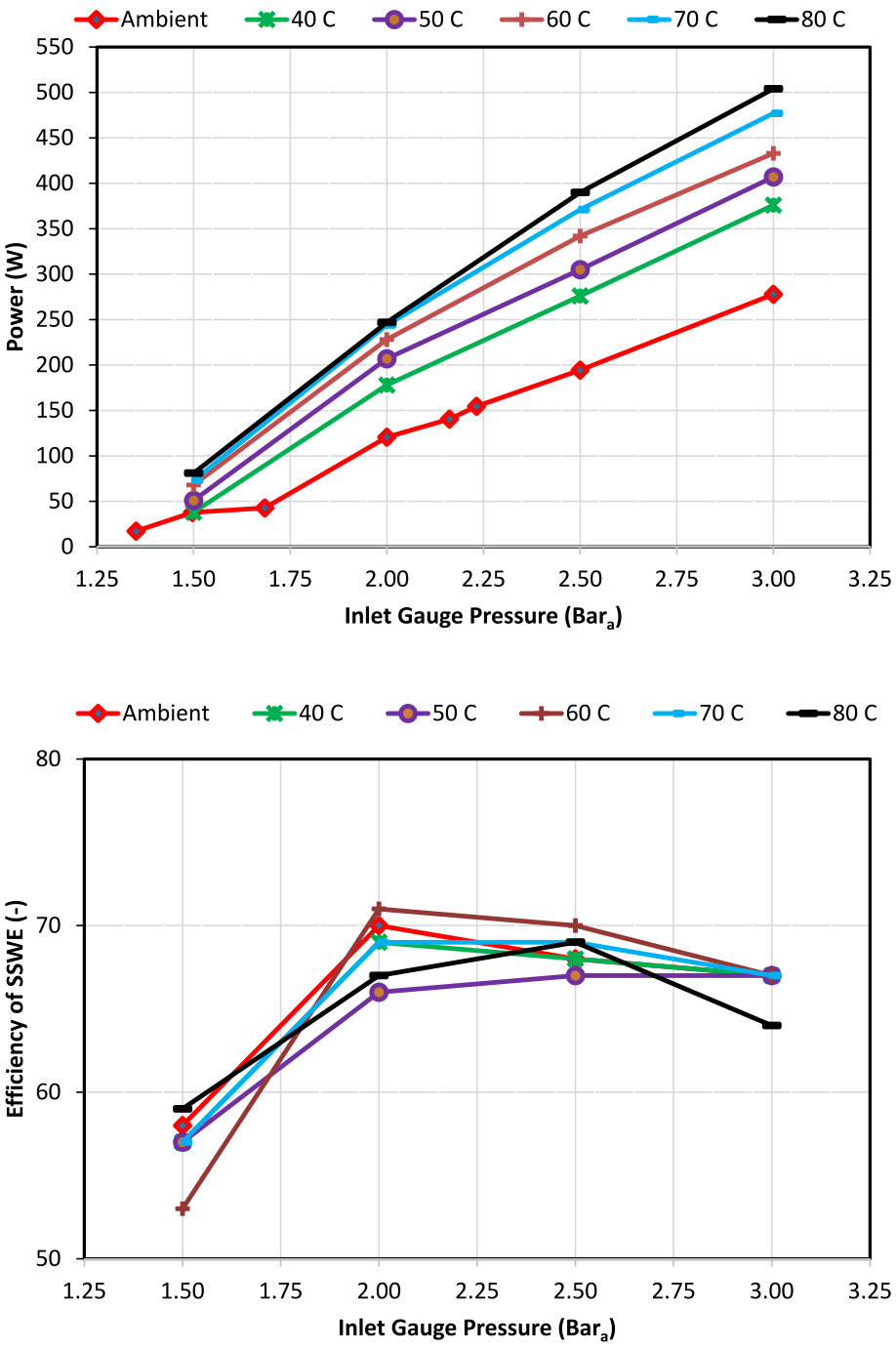

Fig. 7. Experimental results of **a)** power out and **b)** isentropic efficiency from the SSWE.

recorded due to transient region of the data including mass flow data results.

4. SSWE modelling using computational fluid dynamic

Computational fluid dynamics (CFD) is a powerful tool for analyzing the fluid behavior and characteristics in fluid machines and systems before manufacturing. In this work, CFD is utilized to investigate the fluid flow inside the SSWE and study its performance at various inlet pressures and inlet temperatures for micro-scale CAES application. ANSYS Fluent commercial software is employed as it offers a unique tool for dynamic meshing of the complex geometry of the SSWE. In order to simulate the motion of the Wankel expander correctly, user defined functions (UDF) is developed and integrated into Fluent setup to provide the correct mesh movement of all components based on rotational speed. The UDF code was written based on ANSYS Fluent User Guide [46] and the work done by [43]. Fig. 8 explains the main process of CFD simulation of the SSWE.

Firstly, the geometry of the rotor and housing is created using Equation Driven curve tool in SolidWORKS 2022 based on equations 1–5 of the rotor and housing. All chamber bodies are not merged to ensure they are separate bodies when imported to ANSYS Workbench. This means that there is no need to use the ICEM add on tool for combining the mesh file as in previous literature which simplify the meshing process. After the geometry setup, the name selections are created in order to identify the boundary conditions. In the meshing process, tetrahedron mesh is utilised for all geometries as shown in Fig. 9. Finally in the Fluent solver, the setup of boundary conditions are created before

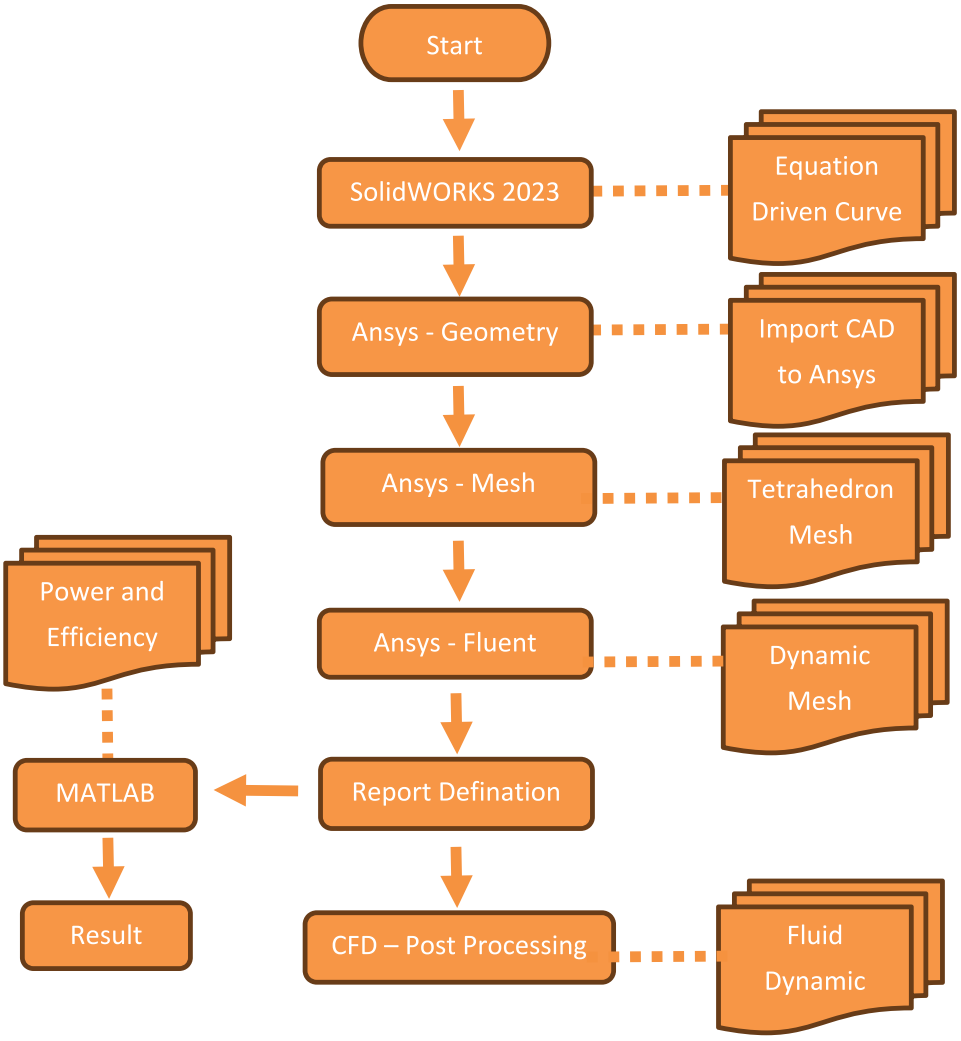

Fig. 8. Flow chart of the CFD simulation setup.

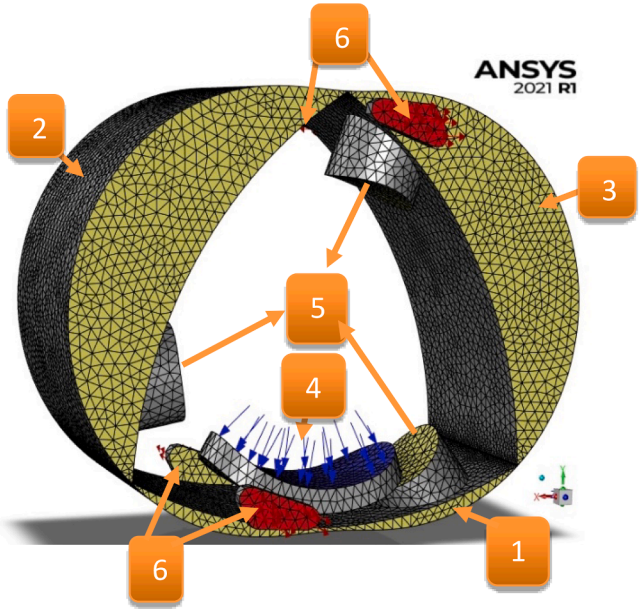

1	2	3
Chamber 1	Chamber 2	Chamber 3
4	**5**	**6**
Inlet	Flanks	Exhaust

Fig. 9. Meshing of the SSWE geometry.

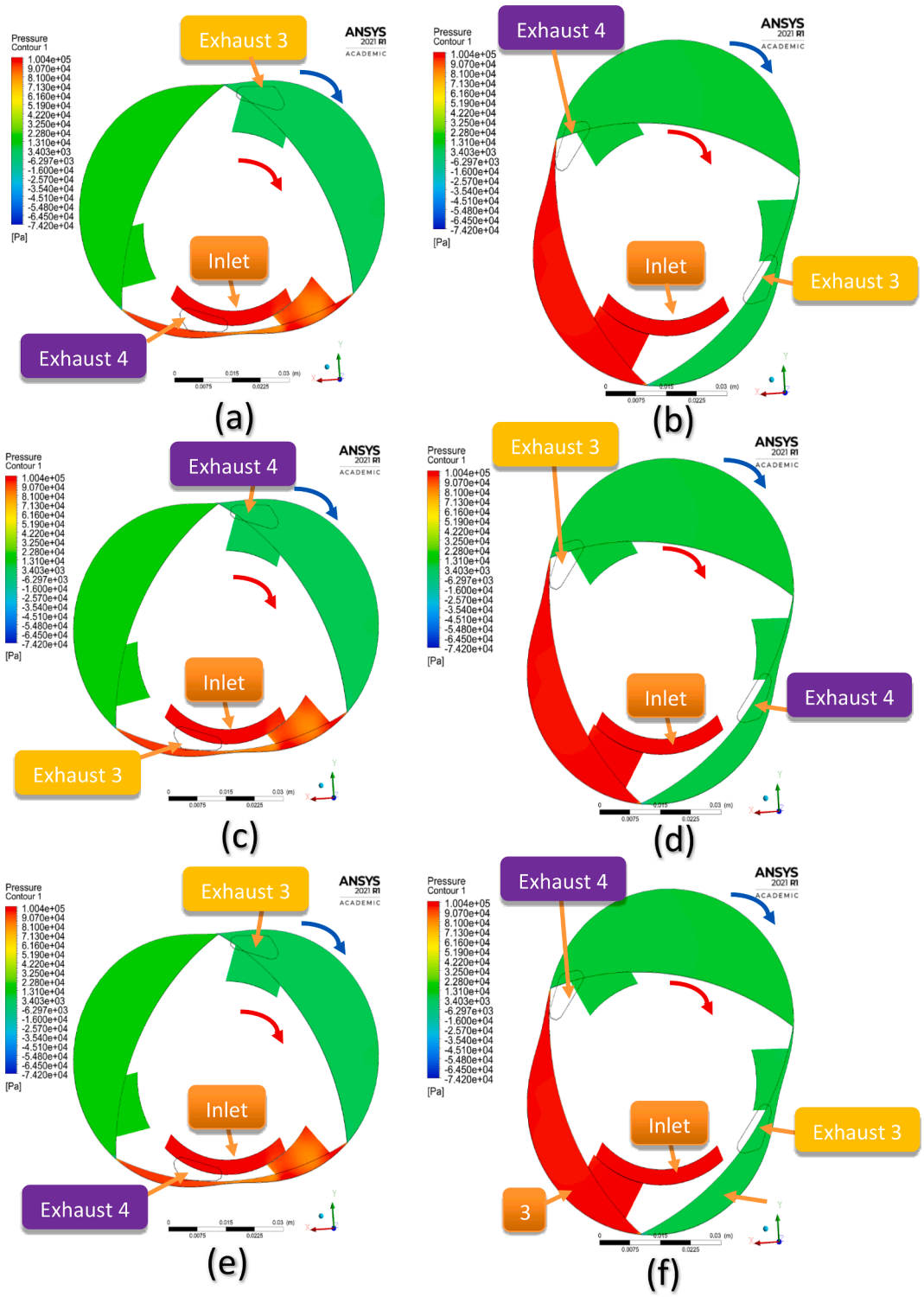

Fig. 10. Pressure distribution of SSWE at inlet pressure 1 bar_g, inlet temperature 300 K, rotational speed 4800 rpm.

running the simulation. In this process, several assumptions are used:

- Pressure-based and transient solvers were chosen (to activate a time-dependent simulation, which is necessary for the simulation of the Wankel expander through a complete cycle).
- For Viscous model, k-epsilon standard model was selected to model turbulent flow.
- Pressure-velocity coupling/ SIMPLE scheme was used for the solution [42,47,48].
- Air as the working fluid.
- The boundary walls are assumed to be adiabatic with no slip.
- For the inlet conditions, Pressure-Inlet (1.5, 2, 2.5 and 3) bar absolute pressure was applied at temperature of 295 K, 330 K, 340 K, 350 K, 360 K and 370 K.
- For the outlet conditions Pressure-outlet (atmospheric pressure) was applied at backflow temperature of 300 K.
- In the UDF code, apply the experimentally measured RPM.

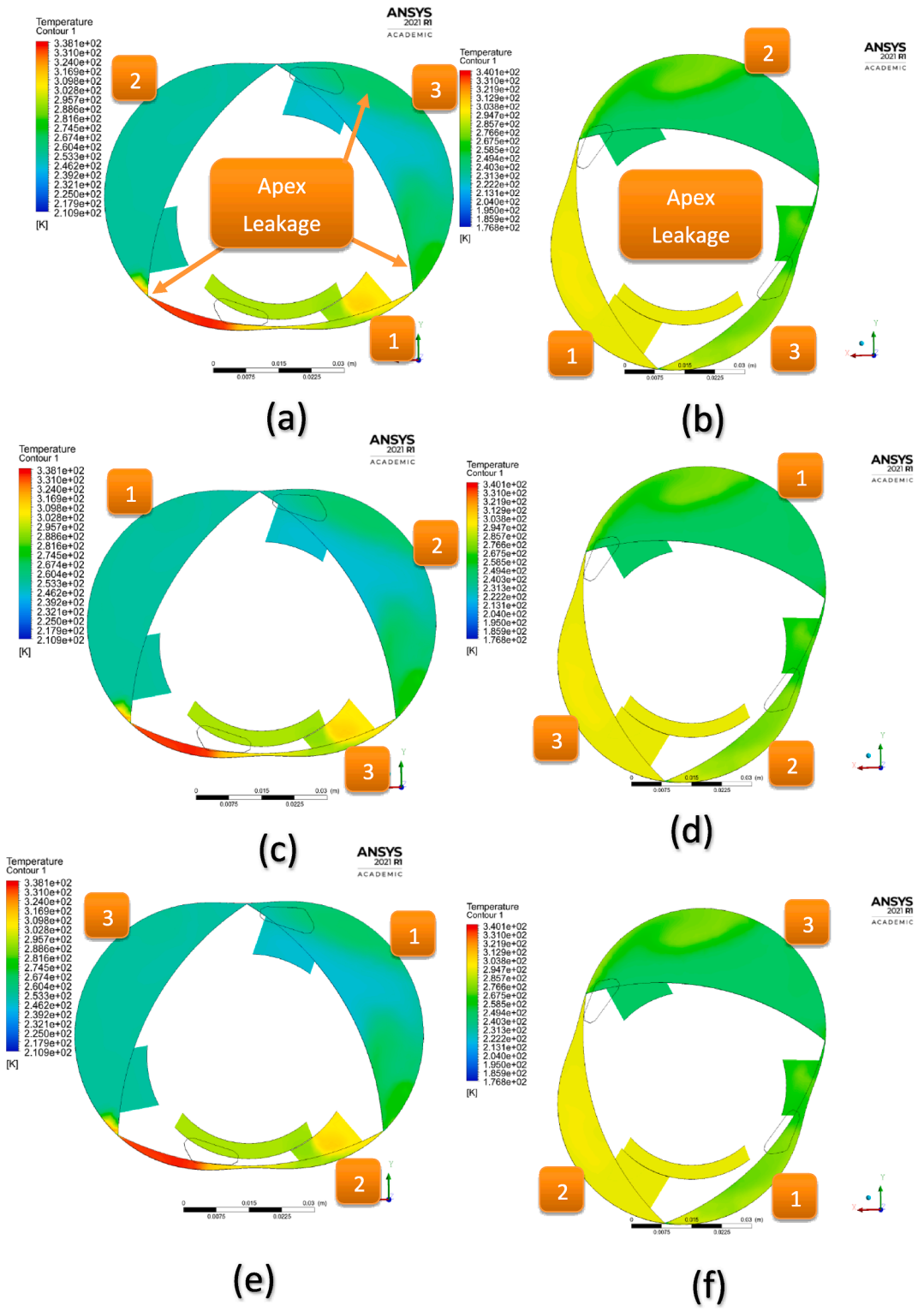

Fig. 11. Temperature distribution of SSWE at inlet pressure 1 bar_g, inlet temperature 300 K, rotational speed 4800 rpm.

Each simulation case takes approximately 120 h using the University of Birmingham's BlueBEAR High Performance Computing service (BHPC) utilising 40 cores. To calculate power output and isentropic efficiency of Wankel expander, several parameters are collected from the report definition results such as mass flow rate, enthalpy, pressure and volume in each chamber and inputted in a MATLAB post processing programme.

Aside from the mesh motion controlled by the UDFs, there are some mesh controls that need to be utilised within the Fluent software itself to maintain the correct mesh shape, size, and quality for accurate results. Local remeshing method only in cell zones that contain tetrahedral or triangular cells. Faces on a deforming boundary are marked for remeshing based on face skewness, minimum and maximum length scale and an optional sizing function. Smoothing and remeshing methods are also used inside all deforming volumes to maintain a good quality, low-skew mesh. Local remeshing method only applies to similar size of mesh in 3D

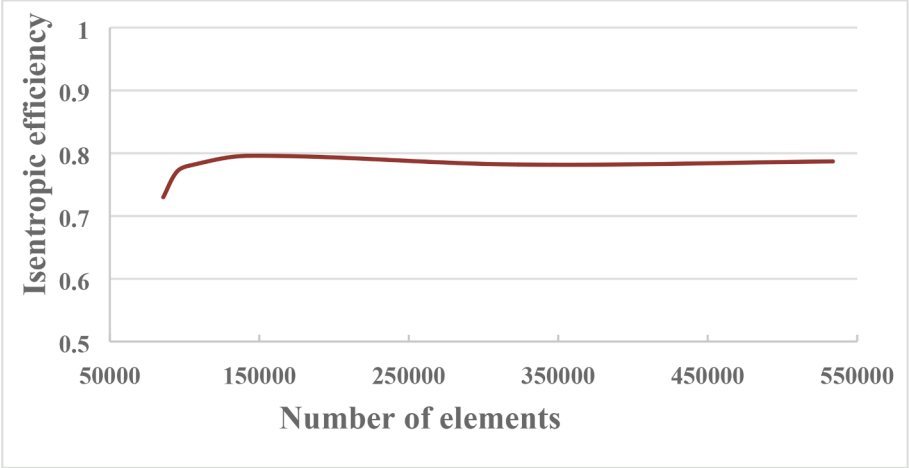

Fig. 12. Mesh sensitivity analysis.

geometries (not a mixed zone) due to UDF. If there was refined mesh in boundary, it would re-meshed according to defined minimum and maximum size of mesh for next timestep. Rotary positive displacement machines mostly are simulated with pre-defined mesh to avoid this issue. However, SSWE is new type expander so there is no available pre-defined meshing software for SSWE. Meshing software pre-generates these numerical meshes of the chambers and gaps for each rotational position and exports the node positions in a set of files. Meshing software ensure that the topology of the meshes keeps the same for each rotational position, i.e. the node numbers and node connectivity remain the same.

Both Fig. 10 and Fig. 11 show that pressure and temperature distrubation of chambers base on the angles in Table 2. The leakage of the clearance can be seen in the edges of the rotor in Fig. 10.

The above case was run using various number of mesh elements to assess the mesh sensitivity of the SSWE CFD simulation. Fig. 13 shows the isentropic efficiency versus the number of elements highlighting that using 150,000 elements is sufficient to produce accurate results.

A mesh sensitivity study consists of running the same simulation using grids with different resolutions and analyzing how much the converged solution changes with each mesh. After running the SSWE simulation for the six different mesh sizes from 2 mm to 0.5 mm and monitoring the parameter of interest result controls. 1.25 mm is chosen for optimum size of mesh.

In the SSWE, each chamber will go through the same thermodynamic cycle. Fig. 13 shows the pressure versus volume diagram of the thermodynamic cycle occurring in each chamber. Fig. 14a shows the volume variation with rotor angle for the three chambers showing that chamber 3 completed one cycle (discharge, compression and exhaust cycle). From angle 0 to 180 has a discharge cycle then angle 180 to 330 is compression cycle and finally exhausted or the completed one cycle at 360. After 17 cm^3, the pressure decreases due to the volume expansion, and this expansion causes the housing and rotor to rotate. Since it is connected to the chamber with the inlet shaft between 1 and 15 cm^3, the pressure remains constant at the applied pressure, even if volume is increased. It allows us to calculate the power the area of under PV diagram. The inlet position has attached with chamber 3. So, the expander is rotated from chamber 3-chamber 1- chamber 2. This is indicated by chamber 3 has completed one cycle compared to chamber 1 and chamber 2. Furthermore, chamber 2 require some time for the next process due to inlet timing after completing the cycle in chamber 3.

Fig. 14 also shows the temperature and pressure variation between inlet and outlet of the SSWE.

Fig. 14 shows the volume, temperature, and pressure variations with housing angle for three chambers showing that each chamber completed one cycle (suction, compression and exhaust) respectively. In Fig. 14a, Chamber 1 is started to suction process due to volume of chamber 1 is increased from 0° to 180°, while volume of chamber 3 is decreased that provide the exhaust process. In order to push the used air, volume of chamber 3 has been decreased and this rotation force comes from the chamber 2 while expansion is occurred. After the 180°, the inlet is connected with chamber 3 starting to suction process during the volume is slightly increased. Between 180° to 360°, volume of chamber 1 is started to expansion due to volume is increased and exhaust port is not connected with chamber 1. After the inlet disconnected with chamber 3, volume of chamber 3 is increased that occur expansion process in chamber 3. When the inlet is connected with chamber 2, volume is the lowest value. Volume of chamber 2 is increased that made a suction process however chamber 3 is started to expansion process while chamber 1 is exhausting between 360° to 540°. In the 540°, all chambers completed the cycle process (suction, expansion and exhaust) and rotor is rotated 360° however housing is rotated 540°. Fig. 12b illustrated inlet temperature is almost constant during the process; however, outlet temperature is changing according to connection of the different chambers. Between 0° to 180°, inlet is connected with chamber 1 and outlet is connected with chamber 3. During the expelling used air, hot air from chamber 2 is leaking to chamber 3 from apex gap. Cold used air is flowing through by exhaust hole meanwhile hot air leakage is filling the chamber 3 until 120o. Between 120° to 180°, exhaust holes are in the middle of the chamber 3 so temperature is suddenly decreased because mostly cold air is expelling through by exhaust port. When the housing angle reached to 180°, volume is the lowest value so most of the mixed cold and hot air is already expelled by exhaust hole, however hot air leakage is continued to leak due to pressure difference. After 180°, chamber 2 is connected with exhaust that's why temperature suddenly decreased to 280 K. Between 180° to 300°, chamber 2 is started to exhaust the used air but leakage from the apex gap is leaking to chamber 1 to chamber 2. After 300°, temperature is sharply decreased due to cold used air, After, 360°, inlet is connected with chamber 2 and chamber 1 started to exhaust process. During the exhaust process, leakage from chamber 3 is entered chamber 1. Exhaust hole is closed the leakage edge so temperature is increased during the expelling from exhaust hole. Between 360° to 540°, same process is continued however the exhaust process was in chamber 1, the suction process in chamber 2 and the expansion process occurred in chamber 3. Therefore the same trend of temperatures can be seen in the Fig. 14b. Fig. 14c shows the pressure variation with housing angle for the three chambers. Inlet is always connected with suction chamber so pressure value is same during the cycle. During the expelling, exhaust chamber is almost same pressure value is connected with ambient. After 45°, there is a slightly decreased fluctuation due to decreased volume during the suction process. Volume of suction chamber is slightly decreased until 45° after that increased sharply to create the suction.

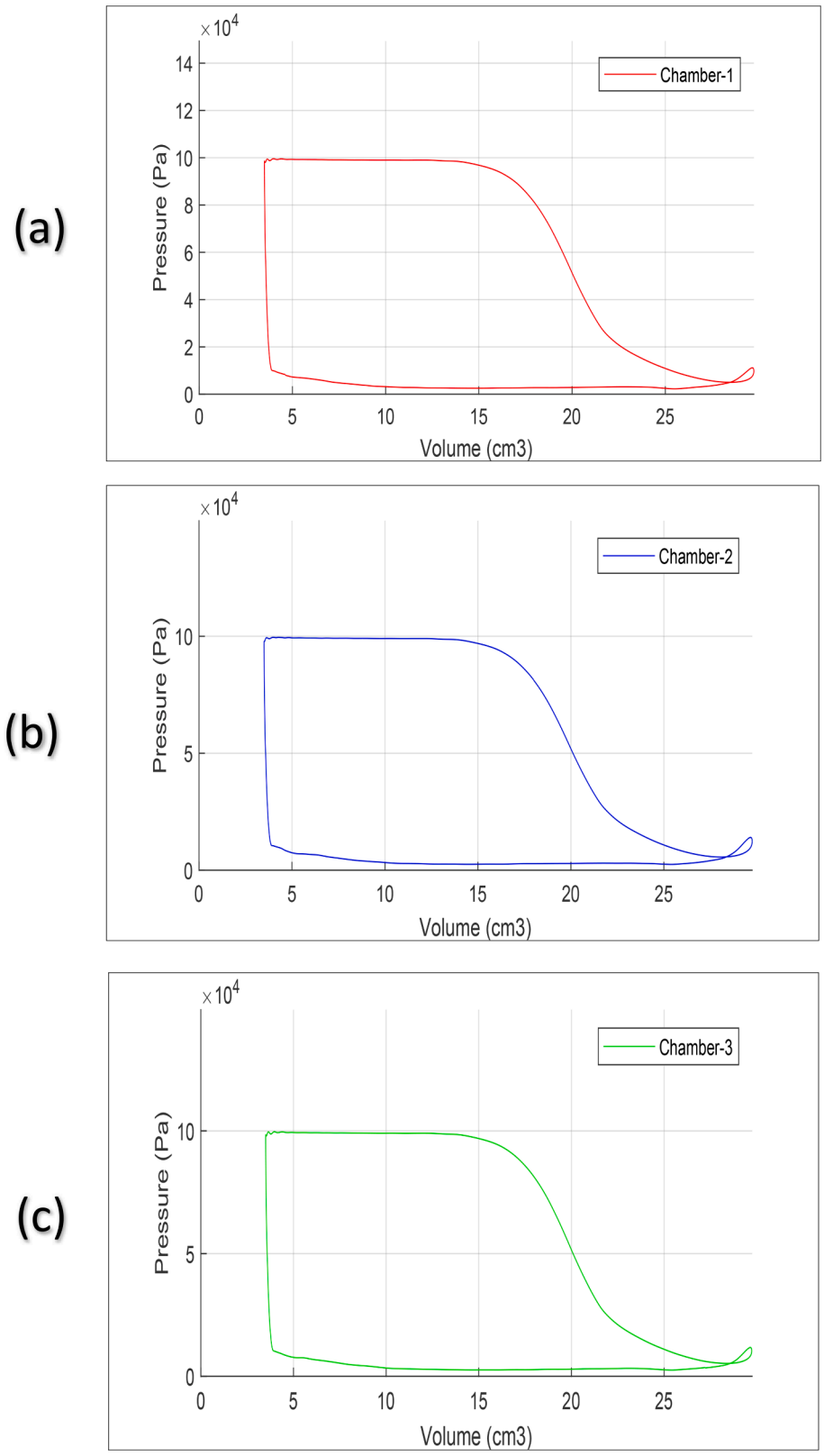

Fig. 13. Pressure versus volume diagram for the three chambers of the SSWE at inlet pressure of 1 bar_g, inlet temperature of 300 K and 4800 rpm.

Fig. 15 depicts the CFD predicted power output and efficiency of the SSWE at inlet temperature raging from ambient to 80 °C and inlet pressure between 1.5 and 3 bar_a. The figure shows that as the inlet pressure and temperature increase, the SSWE CFD power output increases to reach the highest value of 729 Watts at 3 bar_a and 80 °C.

At the same temperature value, there significant increase in the SSWE power output due to the increase in the inlet pressure where at ambient temperature, the SSWE power output increased from 54 Watts to 341 Watts by increasing the pressure from 1.5 to 3 bar_a. On the other hand, at the same pressure value, the increase in power output due to

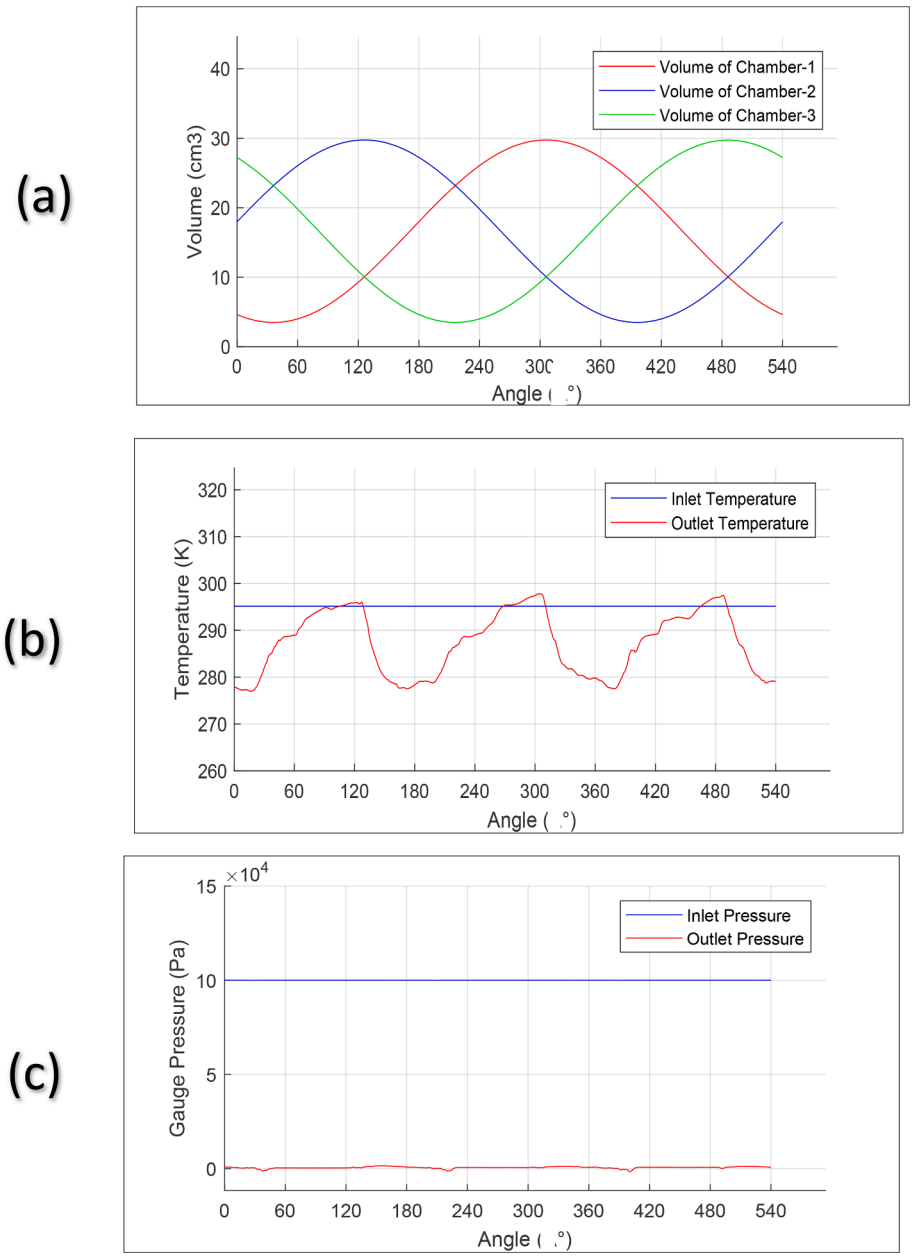

Fig. 14. Chambers' **a)** volume, **b)** temperature and **c)** pressure variation with rotor angle at inlet pressure of 1 bar_g, inlet temperature of 300 K and 4800 rpm.

changes in inlet temperature is less significant where at 2 bar_a, the SSWE power output increased from 106 Watts to 306 Watts by increasing the temperature from ambient to 80 °C. In other words, the inlet pressure was the main parameter that influenced the performance of expander. It is because increasing the inlet pressure results in increasing the rotational speed leading to higher torque and this will increase the power output for all chambers. Fig. 15 also shows that the maximum efficiey occurs at 2 bar_a and temperature of 60 °C. Table 4 compares the CFD predicted poweroutput to those measured experimentally a deviation ranging from 18.2 % to 38.65 %. This difference of deviations due to the fact the CFD simulation do not take into account friction, side leakage (rotor and housing), heat transfer and the limitation of URAN model. Furthermore, in the experiments also had a friction losses of bearing, heat transfer between the expander and air.

Therefore, Fig. 16 shows the power loss plotted versus the inlet pressure at various inlet temperatures.

Fig. 16 presents the power lossaccording to inlet gauge pressure (1.5 bar_a, 2 bar_a, 2.5 bar_a and 3 bar_a) with different temperatures ranging from 20 °C to 80 °C, showing that as temperature and pressure increased lead to the power loss increased. The slightly increased is shown at the temperature of 20 °C whilst the 40 °C to 80 °C showing the same trend of power loss.

Table 5 presents the equations for the power loss as a function of the inlet gauge pressure (x) at various inlet temperatures.

The power loss parameter relied on the inlet pressure an inlet temperature in Table 5. The equations show as the temperature increased lead to the increasing of power loss. It means that in the high temperature of expander resulted in higher power loss.

Improving the CFD accuracy by integrating heat transfer losses modelling and friction equation into the MATLAB post processing to predict all the performance of the static shaft Wankel expander. Furthermore, additional meshing software can be used to export pre-

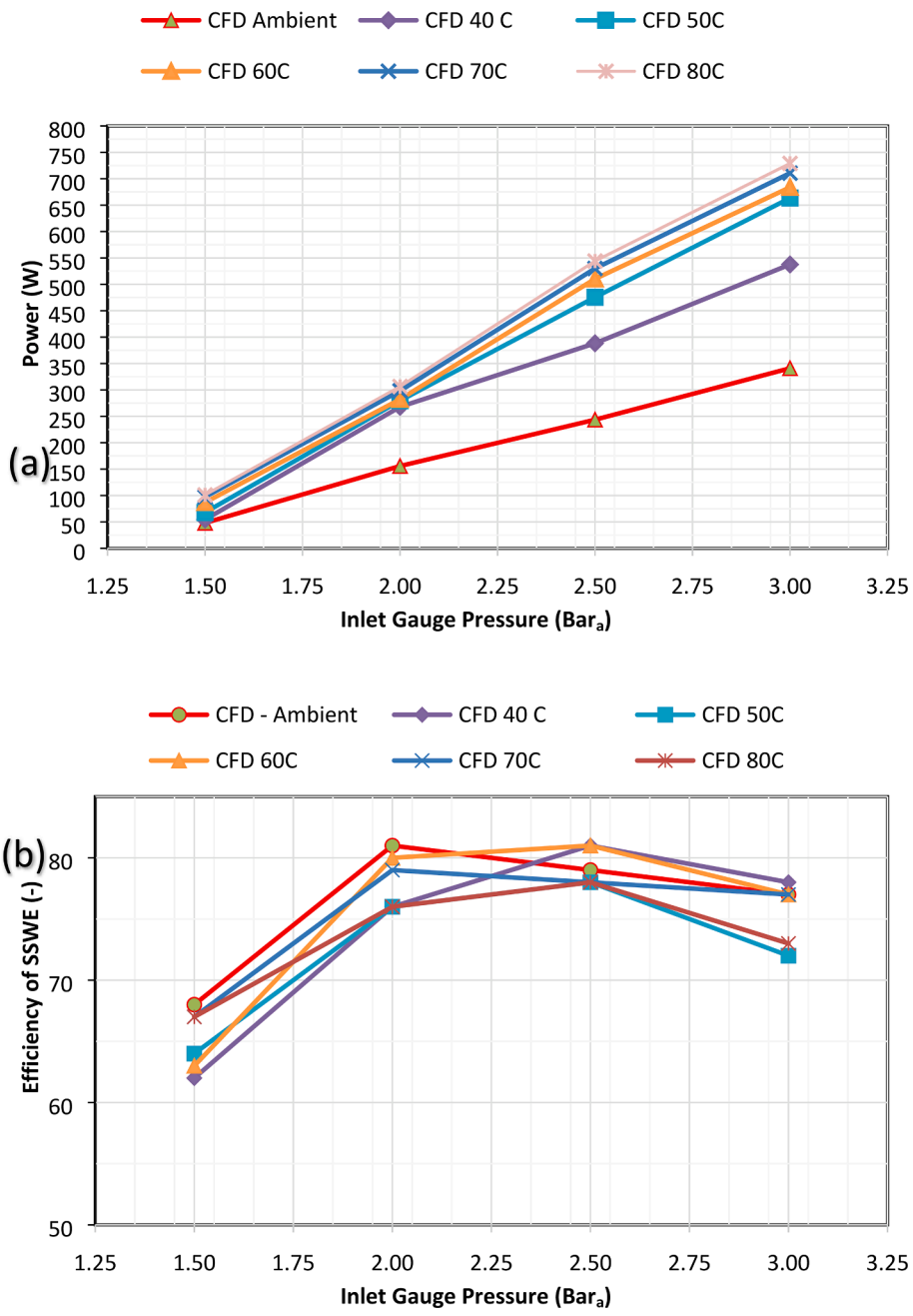

Fig. 15. CFD predicted performance of the SSWE, **(a)** Power output, **(b)** Isentropic efficiency.

Table 4
Comparison of the CFD predicted power output with measured values.

Working Conditions °C Bar	Experiment Watt	CFD Watt	Deviation %
20 1.5	37.72	48.1	21.57
20 2.0	120.69	155.8	22.54
20 2.5	194.39	243.6	20.20
20 3.0	277.79	341.04	18.55
40 1.5	38.0	54.4	30.15
40 2.0	178.0	267.9	33.56
40 2.5	276.0	388.3	28.92
40 3.0	376.0	537.6	30.06
50 1.5	51.0	67.9	24.89
50 2.0	207.0	279.6	25.97
50 2.5	305.0	475.5	35.86
50 3.0	407.0	663.4	38.65
60 1.5	68.0	86.8	21.66
60 2.0	228.0	282.2	19.21
60 2.5	342.0	510.3	32.98
60 3.0	433.0	683.8	36.68
70 1.5	73.0	97.3	24.97
70 2.0	244.0	298.3	18.20
70 2.5	371.0	530	30.00
70 3.0	477.0	710.6	32.87
80 1.5	81.0	101	19.80
80 2.0	247.0	306.4	19.39
80 2.5	390.0	544.1	28.32
80 3.0	504.0	729	30.86

defined files that increases the accuracy of the simulation result by using the ANSYS CFX.

5. Conclusions

Compressed air energy storage is a promising technology for storing surplus energy from intermittent renewable sources and excess overnight electricity. Development of efficient compressed air expander is vital for effective recovery of the stored energy. Static shaft Wankel expander (SSWE) has several advantages including low vibration, ability to produce high power output, low manufacturing cost and requires no valves. This work involves the development of small scale efficient SSWE expander which was experimentally tested using compressed air test rig at various operating pressures (1.5 bar_a to 3 bar_a) and temperatures (20 °C to 80 °C). Also, an advanced computational fluid dynamic simulation model taking into account the dynamic motion of the SSWE and utilising real gas air properties was developed using ANSYS fluent integrated with REFPROP software. The following conclusions can be made:

Experimental testing at temperatures 20 °C to 80 °C and pressures of 1.5 bar_a to 3 bar_a was conducted and showed that as the pressure increases, the power output increases. Also, as the temperature increases, the power output increases. Experimental results showed that the developed SSWE can produce power output of 504 W at 80 °C and 3 bar_a. Results showed that there were a maximum deviation of 38.65 % between experiment and CFD results due to did not cover friction losses, heat transfer losses and side leakage in CFD.

The results of the CFD simulation model were compared to the experimental results showing similar trends but higher values of power output. The difference between the predicted power output and those measured experimentally is due mainly to frictional losses, thus the power loss due to friction was plotted versus the inlet gauge pressure. Equations were then obtained for the power loss as a function of the inlet gauge pressure. As the inlet temperature and pressure increase, the power loss increases.

Practically, to improve the power output and overall efficiency, leakage losses has to be eliminated and friction losses has to be reduced. In this work, leakage losses were eliminated by using the right seals for the outside casing and countersunk head bolts configuration to achieve tight coupling. Improving the static shaft support by adding another bearing have reduced static shaft oscilation and eliminated the rotor edges touching the housing therefore significantly reduce frictional losses and improved the power output.

Table 5
Power loss equation at various inlet temperature.

Temperature	Equation
40 °C	$-286.2*x^4 + 952.97*x^3-814.2*x^2 + 237.3*x$
50 °C	$57.6*x^4-213.93*x^3-301.2*x^2-72.26*x$
60 °C	$292.4*x^4-949.7*x^3 + 918.6*x^2-227.07*x$
70 °C	$293.8*x^4-928.37*x^3 + 888.6*x^2-219.73*x$
80 °C	$115*x^4-377.13*x^3 + 427*x^2-105.47*x$

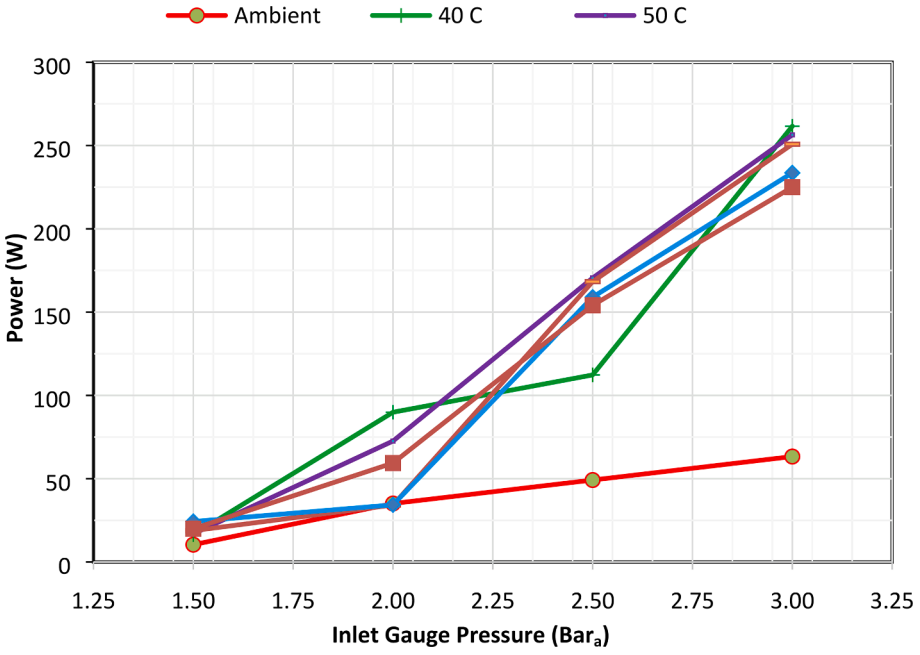

Fig. 16. Power loss.

To improve the CFD accuracy by integrating heat transfer losses modelling and friction equation into the MATLAB post processing to predict the performance of the static shaft Wankel expander similar condition with experiment. Furthermore, additional meshing software can be used to export pre-defined files that increases the accuracy of the simulation result by using the ANSYS CFX.

CRediT authorship contribution statement

Jonri LomiGa: Conceptualization, Methodology, Data curation, Writing – original draft, Investigation, Writing – review & editing. **Anil Taskin:** Conceptualization, Methodology, Data curation, Visualization, Investigation, Writing – review & editing. **Raya Al-Dadah:** Supervision, Validation, Writing – review & editing, Project administration, Resources. **Saad Mahmoud:** Supervision, Project administration, Writing – review & editing. **Andrew N. Aziz:** .

Declaration of Competing Interest

The authors declare that they have no known competing financial interests or personal relationships that could have appeared to influence the work reported in this paper.

Data availability

No data was used for the research described in the article.

Acknowledgement

This work was supported by the Indonesian Endowment Fund for Education (LPDP), Ministry of Finance, Republic of Indonesia, grant no. 201804220112690 and the University of Birmingham for providing the University of Birmingham's BlueBEAR HPC service, which provides a High Performance Computing service to the University's research community.

References

[1] Iea. Key World Energy Statistics 2021 – Statistics Report. IEA Publ; 2021. p. 1–82.
[2] Ahmad T, Zhang D. A critical review of comparative global historical energy consumption and future demand: The story told so far. Energy Rep 2020;6:1973–91. https://doi.org/10.1016/j.egyr.2020.07.020.
[3] Wang F, et al. Technologies and perspectives for achieving carbon neutrality. Innovation 2021;2(4):pp. https://doi.org/10.1016/j.xinn.2021.100180.
[4] Rabi A, Radulovic J, Buick J. Comprehensive Review of Compressed Air Energy Storage (CAES) Technologies. Thermo 2023;3(1):104–26. https://doi.org/10.3390/thermo3010008.
[5] King M, Jain A, Bhakar R, Mathur J, Wang J. Overview of current compressed air energy storage projects and analysis of the potential underground storage capacity in India and the UK. Renew Sustain Energy Rev 2021;vol. 139, no. January:110705. https://doi.org/10.1016/j.rser.2021.110705.
[6] Salvini C, Giovannelli A. Techno-economic comparison of diabatic CAES with artificial air reservoir and battery energy storage systems. Energy Rep 2022;8:601–7. https://doi.org/10.1016/j.egyr.2022.03.170.
[7] Al-Zareer M, Dincer I, Rosen MA. Development and analysis of a portable compressed liquid air cooling system for fast vehicle cabin cooling. Int J Refrig 2017;84:117–27. https://doi.org/10.1016/j.ijrefrig.2017.09.004.
[8] S. Farrukh, D. Wu, R. Al-Dadah, W. Gao, and Z. Wang, "A review of integrated cryogenic energy assisted power generation systems and desalination technologies," *Appl. Therm. Eng.*, vol. 221, no. December 2022, p. 119836, 2023, doi: 10.1016/j.applthermaleng.2022.119836.
[9] Bazdar E, Sameti M, Nasiri F, Haghighat F. Compressed air energy storage in integrated energy systems: A review. Renew Sustain Energy Rev 2022;vol. 167, no. July:112701. https://doi.org/10.1016/j.rser.2022.112701.
[10] A. G. Olabi, T. Wilberforce, M. Ramadan, M. A. Abdelkareem, and A. H. Alami, "Compressed air energy storage systems: Components and operating parameters – A review," *J. Energy Storage*, vol. 34, no. August 2020, p. 102000, 2021, doi: 10.1016/j.est.2020.102000.
[11] Wasbari F, Bakar RA, Gan LM, Tahir MM, Yusof AA. A review of compressed-air hybrid technology in vehicle system. Renew Sustain Energy Rev 2017;67:935–53. https://doi.org/10.1016/j.rser.2016.09.039.
[12] Verma SS. Latest Developments of a Compressed Air Vehicle: A Status Report Latest Developments of a Compressed Air Vehicle A Status Report Latest Developments of a Compressed Air Vehicle: A Status Report. Glob J Res Eng Automot Eng 2013;13.
[13] Y. Fang, Y. Lu, A. P. Roskilly, and X. Yu, "A review of compressed air energy systems in vehicle transport," *Energy Strateg. Rev.*, vol. 33, no. November 2020, p. 100583, 2021, doi: 10.1016/j.esr.2020.100583.
[14] Nabil T. Investigation and implementation of compressed air powered motorbike engines. Eng Reports 2019;1(2):1–13. https://doi.org/10.1002/eng2.12034.
[15] E. Bazdar, F. Nasiri, and F. Haghighat, "An improved energy management operation strategy for integrating adiabatic compressed air energy storage with renewables in decentralized applications," *Energy Convers. Manag.*, vol. 286, no. November 2022, p. 117027, 2023, doi: 10.1016/j.enconman.2023.117027.
[16] S. Sarmast, K. Rouindej, R. A. Fraser, and M. B. Dusseault, "Sizing-design method for compressed air energy storage (CAES) systems: A case study based on power grid in Ontario," *Energy Convers. Manag.*, vol. 277, no. September 2022, p. 116656, 2023, doi: 10.1016/j.enconman.2023.116656.
[17] He W, Wang J. Optimal selection of air expansion machine in Compressed Air Energy Storage: A review. Renew Sustain Energy Rev 2018;87(January):77–95. https://doi.org/10.1016/j.rser.2018.01.013.
[18] Zhi R, Lei B, Zhang C, Ji W, Wu Y. Experimental study of single screw expander with different oil-gas separators in compressed air powered system. Energy 2021;235:121371. https://doi.org/10.1016/j.energy.2021.121371.
[19] He W, Wu Y, Peng Y, Zhang Y, Ma C, Ma G. Influence of intake pressure on the performance of single screw expander working with compressed air. Appl Therm Eng 2013;51(1–2):662–9. https://doi.org/10.1016/j.applthermaleng.2012.10.013.
[20] Lu Y, He W, Wu Y, Ji W, Ma C, Guo H. Performance study on compressed air refrigeration system based onsingle screw expander. Energy 2013;55:762–8. https://doi.org/10.1016/j.energy.2013.03.051.
[21] Xinghua Y, Jidai W, Jiazhen P, Xinjun L. Mathematical modeling and experimental research on scroll expander. Appl Mech Mater 2012;229–231:1900–3. https://doi.org/10.4028/www.scientific.net/AMM.229-231.1900.
[22] Zhang X, et al. Study on the performance and optimization of a scroll expander driven by compressed air. Appl Energy 2017;186:347–58. https://doi.org/10.1016/j.apenergy.2016.06.004.
[23] Guangbin L, Yuanyang Z, Liansheng L, Pengcheng S. Simulation and experiment research on wide ranging working process of scroll expander driven by compressed air. Appl Therm Eng 2010;30(14–15):2073–9. https://doi.org/10.1016/j.applthermaleng.2010.05.015.
[24] Tenissara N, Thepa S, Monyakul V. Performance study of a small-single piston expander using compressed air as working fluid. Energy Procedia 2017;138:610–5. https://doi.org/10.1016/j.egypro.2017.10.169.
[25] Huang CY, Hu CK, Yu CJ, Sung CK. Experimental investigation on the performance of a compressed-air driven piston engine. Energies 2013;6(3):1731–45. https://doi.org/10.3390/en6031731.
[26] Al Jubori AM, Jawad QA. Investigation on performance improvement of small scale compressed-air energy storage system based on efficient radial-inflow expander configuration. Energy Convers Manag 2019;182(January):224–39. https://doi.org/10.1016/j.enconman.2018.12.048.
[27] Khalil KM, Mahmoud S, Al- Dadah RK. Experimental and numerical investigation of blade height effects on micro-scale axial turbines performance using compressed air open cycle. Energy 2020;211:118660. https://doi.org/10.1016/j.energy.2020.118660.
[28] Z. Yuqiao, L. W. Lam, and L. Thong-See, "2D Cfd Modeling of a Pump With Wankel Rotary Engine Geometry," *11th Int. Conf. Fluid Mach.*, no. November 2011, 2011.
[29] Ogura I. The Ogura-Wankel compressor - Application of Wankel rotary concept as automotive air conditioning compressor. SAE Tech Pap 1982. https://doi.org/10.4271/820159.
[30] Garside DW. A new Wankel-type compressor and vacuum pump. IOP Conf. Ser Mater Sci Eng 2017;232(1):pp. https://doi.org/10.1088/1757-899X/232/1/012065.
[31] J. Spreitzer, F. Zahradnik, and B. Geringer, "Implementation of a Rotary Engine (Wankel Engine) in a CFD Simulation Tool with Special Emphasis on Combustion and Flow Phenomena," *SAE Tech. Pap.*, vol. 2015-April, no. April, 2015, doi: 10.4271/2015-01-0382.
[32] C. Ji, H. Wang, C. Shi, S. Wang, and J. Yang, "Multi-objective optimization of operating parameters for a gasoline Wankel rotary engine by hydrogen enrichment," *Energy Convers. Manag.*, vol. 229, no. August 2020, p. 113732, 2021, doi: 10.1016/j.enconman.2020.113732.
[33] Amrouche F, Erickson PA, Varnhagen S, Park JW. An experimental study of a hydrogen-enriched ethanol fueled Wankel rotary engine at ultra lean and full load conditions. Energy Convers Manag 2016;123:174–84. https://doi.org/10.1016/j.enconman.2016.06.034.
[34] Fan B, Pan J, Tang A, Pan Z, Zhu Y, Xue H. Experimental and numerical investigation of the fluid flow in a side-ported rotary engine. Energy Convers Manag 2015;95:385–97. https://doi.org/10.1016/j.enconman.2015.02.047.
[35] Badr O, Naik S, O'Callaghan PW, Probert SD. Expansion machine for a low power-output steam Rankine-cycle engine. Appl Energy 1991;39(2):93–116. https://doi.org/10.1016/0306-2619(91)90024-R.
[36] Badr O, Naik S, O'Callaghan PW, Probert SD. Rotary Wankel engines as expansion devices in steam Rankine-cycle engines. Appl Energy 1991;39(1):59–76. https://doi.org/10.1016/0306-2619(91)90063-4.
[37] Antonelli M, Baccioli A, Francesconi M, Desideri U, Martorano L. Operating maps of a rotary engine used as an expander for micro-generation with various working fluids. Appl Energy 2014;113:742–50. https://doi.org/10.1016/j.apenergy.2013.08.003.
[38] Antonelli M, Baccioli A, Francesconi M, Martorano L. Experimental and numerical analysis of the valve timing effects on the performances of a small volumetric rotary expansion device. Energy Procedia 2014;45:1077–86. https://doi.org/10.1016/j.egypro.2014.01.113.

[39] Francesconi M, Antonelli M. A numerical model for the prediction of the fluid dynamic and mechanical losses of a Wankel-type expansion device. Appl Energy 2017;205(August):225–35. https://doi.org/10.1016/j.apenergy.2017.07.125.
[40] Sadiq GA, Tozer G, Al-Dadah R, Mahmoud S. CFD simulations of compressed air two stage rotary Wankel expander – Parametric analysis. Energy Convers Manag 2017;142:42–52. https://doi.org/10.1016/j.enconman.2017.03.040.
[41] G. A. Sadiq, "Development of compressed air rotary Wankel devices for hybrid vehicle," no. January, 2018, [Online]. Available: https://etheses.bham.ac.uk/id/eprint/8211/.
[42] G. Tozer, R. Al-Dadah, and S. Mahmoud, "Simulating apex gap sizes in a small scale Wankel expander for air liquefaction," *Appl. Therm. Eng.*, vol. 154, no. December 2018, pp. 476–484, 2019, doi: 10.1016/j.applthermaleng.2019.03.085.
[43] G. Tozer, "Development of a static shaft wankel expander for small-scale applications by," no. June, p. 371, 2020, [Online]. Available: https://etheses.bham.ac.uk/id/eprint/11130/.
[44] Sadiq GA, Al-Dadah R, Mahmoud S. Development of rotary Wankel devices for hybrid automotive applications. Energy Convers Manag 2019;vol. 202, no. October:112159. https://doi.org/10.1016/j.enconman.2019.112159.
[45] K. Yamamoto, *Rotary engine: Sankaido*. 1981.
[46] *Ansys Fluent Theory Guide, Release 2021*. ANSYS, Inc., 2021.
[47] Hsieh CF. Dynamics analysis of the triangular rotary engine structures. J Eng Gas Turbines Power 2018;140(11):pp. https://doi.org/10.1115/1.4039810.
[48] Hsieh CF, Chen KT, Johar T. Fluid flow characteristics of two types rotary engines. Int J Hydrogen Energy 2021;46(80):40154–74. https://doi.org/10.1016/j.ijhydene.2021.09.250.